



HAL
open science

CSB-Dependent Cyclin-Dependent Kinase 9 Degradation and RNA Polymerase II Phosphorylation during Transcription-Coupled Repair

Lise-Marie Donnio, Anna Lagarou, Gabrielle Sueur, Pierre-Olivier Mari,
Giuseppina Giglia-Mari

► **To cite this version:**

Lise-Marie Donnio, Anna Lagarou, Gabrielle Sueur, Pierre-Olivier Mari, Giuseppina Giglia-Mari. CSB-Dependent Cyclin-Dependent Kinase 9 Degradation and RNA Polymerase II Phosphorylation during Transcription-Coupled Repair. *Molecular and Cellular Biology*, 2019, 39 (6), 10.1128/mcb.00225-18 . hal-03843799

HAL Id: hal-03843799

<https://hal.science/hal-03843799>

Submitted on 9 Nov 2022

HAL is a multi-disciplinary open access archive for the deposit and dissemination of scientific research documents, whether they are published or not. The documents may come from teaching and research institutions in France or abroad, or from public or private research centers.

L'archive ouverte pluridisciplinaire **HAL**, est destinée au dépôt et à la diffusion de documents scientifiques de niveau recherche, publiés ou non, émanant des établissements d'enseignement et de recherche français ou étrangers, des laboratoires publics ou privés.



CSB-Dependent Cyclin-Dependent Kinase 9 Degradation and RNA Polymerase II Phosphorylation during Transcription-Coupled Repair

Lise-Marie Donnio,^a Anna Lagarou,^a Gabrielle Sueur,^b Pierre-Olivier Mari,^a  Giuseppina Giglia-Mari^a

^aInstitut NeuroMyoGène (INMG), CNRS UMR 5310, INSERM U1217, Université de Lyon, Université Claude Bernard Lyon 1, Villeurbanne, France

^bCNRS, IPBS (Institut de Pharmacologie et de Biologie Structurale), Toulouse, France

ABSTRACT DNA lesions block cellular processes such as transcription, inducing apoptosis, tissue failures, and premature aging. To counteract the deleterious effects of DNA damage, cells are equipped with various DNA repair pathways. Transcription-coupled repair specifically removes helix-distorting DNA adducts in a coordinated multistep process. This process has been extensively studied; however, once the repair reaction is accomplished, little is known about how transcription restarts. In this study, we show that, after UV irradiation, the cyclin-dependent kinase 9 (CDK9)/cyclin T1 kinase unit is specifically released from the HEXIM1 complex and that this released fraction is degraded in the absence of the Cockayne syndrome group B protein (CSB). We determine that UV irradiation induces a specific Ser2 phosphorylation of the RNA polymerase II and that this phosphorylation is CSB dependent. Surprisingly, CDK9 is not responsible for this phosphorylation but instead might play a nonenzymatic role in transcription restart after DNA repair.

KEYWORDS CDK9, DNA repair, RNAP2, nucleotide excision repair, transcription, transcription-coupled repair

Cells are the units of organic life and store in their nuclei, under the form of the DNA molecule, what constitutes the instruction manual for proper cellular functioning. Despite the protection offered by the cellular environment, the integrity of DNA is continuously challenged by a variety of endogenous and exogenous agents (e.g., UV light, cigarette smoke, environmental pollution, oxidative damage, etc.) that cause DNA lesions, interfering with proper cellular functions, *in fine* causing the aging or premature aging of the tissue and later on of the whole organism.

To prevent the deleterious consequences of persisting DNA lesions, all organisms are equipped with a network of efficient DNA damage responses and DNA repair systems. One of these systems is called nucleotide excision repair (NER). NER removes helix-distorting DNA adducts such as UV-induced lesions (cyclopyrimidine dimers and 6-4 photoproducts) in a coordinated multistep process (1).

NER exists in two distinct subpathways depending upon where DNA lesions are located within the genome. Global genome repair (GGR) will predominantly repair DNA lesions located on nontranscribed DNA, whereas the second subpathway, transcription-coupled repair (TCR), is directly coupled to transcription elongation and repairs DNA lesions located on the transcribed strand of active genes.

RNA polymerase II (RNAP2) frequently encounters transcription-blocking DNA lesions that need to be removed through the TCR process before resumption of transcription can take place (2). Constant obstruction of transcription has severe consequences for the cell, as it might also be a signal for apoptosis. Deficient TCR is illustrated in Cockayne syndrome (CS) patients; CS is a rare inherited syndrome char-

Citation Donnio L-M, Lagarou A, Sueur G, Mari P-O, Giglia-Mari G. 2019. CSB-dependent cyclin-dependent kinase 9 degradation and RNA polymerase II phosphorylation during transcription-coupled repair. *Mol Cell Biol* 39:e00225-18. <https://doi.org/10.1128/MCB.00225-18>.

Copyright © 2019 American Society for Microbiology. All Rights Reserved.

Address correspondence to Giuseppina Giglia-Mari, ambra.mari@univ-lyon1.fr.

Received 7 May 2018

Returned for modification 31 May 2018

Accepted 14 December 2018

Accepted manuscript posted online 2 January 2019

Published 1 March 2019

acterized by multisystem clinical malfunctions, growth and neurological abnormalities and features of premature aging due to increased apoptosis. At the cellular level, a hallmark of CS is the inability to resume RNA synthesis after exposure to UV light (3–5). This not only identifies TCR as a crucial defense mechanism against DNA damage for cells and organisms to evade the lethal effects of transcription hindrance but also highlights the great importance of transcription resumption after repair of the damaged transcribed strand.

During a TCR event, two phases can be distinguished: (i) the actual repair of the damaged strand via the TCR subpathway and (ii) the resumption of transcription after repair (RTR). Although the TCR repair process has been extensively described, the molecular mechanisms implicated in RTR and the specific proteins involved are still elusive. The regulation of resumption of transcription after repair is highly important given that improper restart leads to cellular malfunction and apoptosis and concomitantly contributes to aging.

Interestingly, there has been some recent progress concerning the complex, yet poorly defined, mechanism that allows transcription resumption after DNA repair. These studies opened the way for a deeper understanding of the RTR mechanism at different levels (6–9). One of these studies identifies ELL (eleven-nineteen lysine-rich leukemia), an RNAP2 elongation factor, as a new partner of the basal transcription repair factor TFIIH (7). The best-characterized function of ELL is to increase the catalytic rate of RNAP2 transcription by suppressing transient pausing of the polymerase at multiple sites along the DNA during elongation (10). The combination of the UV sensitivity, the absence of RNA recovery synthesis (RRS), and the proficient unscheduled DNA synthesis (UDS), illustrated in ELL-depleted cells upon UV irradiation, suggests that ELL is an indirect TCR factor that plays a more specific role during RTR. To date, these results favor a possible model wherein ELL is recruited to the lesion-arrested RNAP2 by its interaction with TFIIH and functions as a platform for the recruitment of other elongation factors in order to facilitate RTR (7).

Several groups have reported *in vitro* that ELL and the positive transcription elongation factor b (P-TEFb) are found together with several mixed-lineage leukemia (MLL) translocation partners in so-called super elongation complexes (11). P-TEFb consists of a heterodimeric kinase, composed of cyclin-dependent kinase 9 (CDK9) and its cyclins T1 and T2, which play a central role in the release of RNAP2 from pausing. In mammalian cells, the CDK9 subunit of P-TEFb phosphorylates RNAP2 at its Ser-2 carboxy-terminal domain (CTD) repeat to license the assembly of multiple factors critical for mRNA biogenesis, chromatin modifications during transcription (12), and the marking of transcription elongation (13). Interestingly, phosphorylation of the CTD does not directly affect elongation rate but instead mediates interactions between the polymerase and other factors (14). Therefore, the Ser5P-to-Ser2P transition could either promote the association and activity of positive elongation factors or inhibit pathways that cause RNAP2 to pause or terminate early in elongation. Hence, it is possible that ELL functions via its interaction with P-TEFb and its subsequent recruitment in order to facilitate transcriptional resumption after repair of a transcription blocking DNA lesion.

We investigated the role of CDK9 during TCR and most precisely during RTR. Our results show that CDK9 plays a role in the TCR reaction and that its absence delays but does not inhibit transcription restart completely. Interestingly, we could highlight a DNA damage-dependent dissociation of CDK9 and cyclins T from the 75K snRNP complex and a degradation of CDK9 and cyclins T after UV irradiation in TCR-deficient cells. Finally, we show that during RTR the RNAP2 is unambiguously phosphorylated at the Ser2 position (independently from CDK9 kinase activity) and that this phosphorylation is absent in TCR-deficient cells.

RESULTS

CDK9 function during global genome repair. Because of the strong relation between ELL and CDK9 (11), we decided to explore the role of CDK9 in DNA repair and particularly within the GGR/TCR NER system.

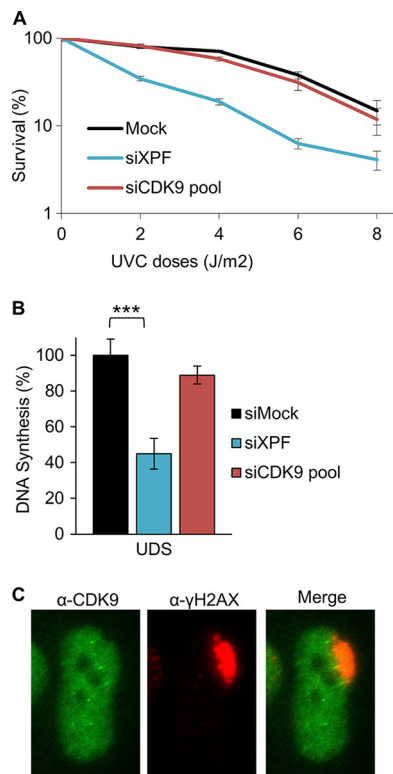


FIG 1 CDK9 function during global genome repair. (A) Sensitivity to UV-C of SV-40 immortalized human fibroblast MRC5 cells (MRC5 cells) treated with siRNA against the indicated factors, as determined by colony-forming ability. (B) UDS determined by EdU incorporation after local UV-C exposure in MRC5 cells after siRNA-mediated knockdown of the indicated factors. At least 20 nuclei were analyzed. (C) Immunofluorescence staining of MRC5 cells with anti-CDK9 and anti- γ H2AX antibody 3 h after local damage induction with UV-C.

Repressing CDK9 expression by small interfering RNA (siRNA) in normal human MRC5 fibroblasts led to no UV-specific cytotoxicity, comparable to mock-knocked-down cells, as measured by clonogenic survival (Fig. 1A). As a positive control, the knockdown of the well-known NER endonuclease XPF (xeroderma pigmentosum complementation group F protein) was used, which, as expected, produced severe UV cytotoxicity. This result clearly indicates that CDK9 absence does not confer UV sensitivity to cells.

Although cell survival after UV treatment is a general measure of the cellular DNA repair activity, the gold standard to quantify GGR activity is the unscheduled DNA synthesis after UV treatment. This assay quantifies DNA replication after repair, i.e., the refilling of single-strand DNA gaps generated by NER processing of UV-induced DNA lesions within locally UV-exposed cell nuclei. As expected for NER-deficient cells unable to process UV lesions, XPF siRNA-treated cells showed a strong reduction in UDS levels (Fig. 1B). CDK9-depleted cells showed no significant decrease in UDS levels, as in mock-knocked-down cells, suggesting that CDK9 is not an essential factor during GGR. In addition, no endogenous CDK9 local damage accumulation was observed when MRC5 cells were locally UV irradiated (Fig. 1C).

CDK9 function during transcription restart after DNA repair. These results show that CDK9 is not involved in the GGR subpathway but do not exclude that CDK9, as hypothesized by its role within transcription, could be involved in TCR and RTR. In fact, proteins involved in TCR are not easily visualized on the damage areas. This is mainly due to the low level of TCR (10%) versus GGR (90%) in the cells (7) and intrinsically because the TCR reactions are primarily related to the transcribed genes, their number is thus limited to the number of active transcriptions.

The gold standard assay to measure TCR activity in the cell is the RNA recovery synthesis (RRS) assay. In this assay, transcriptional activity is visualized by detecting and

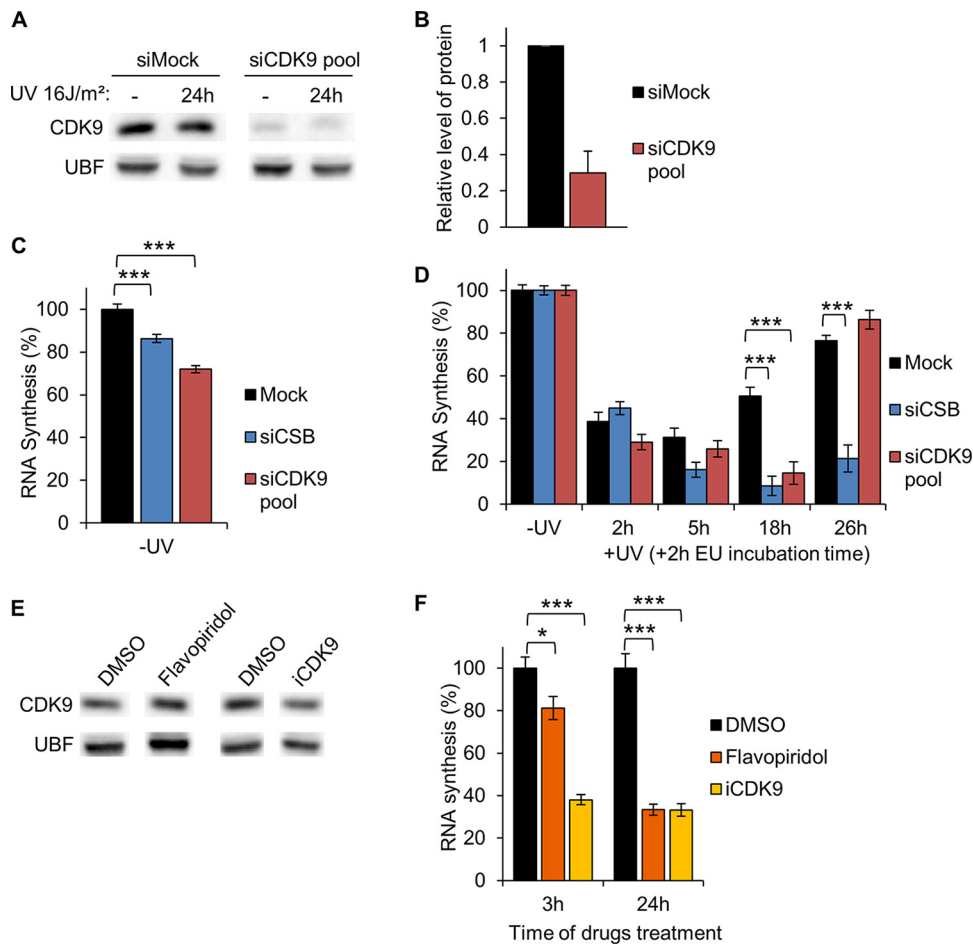


FIG 2 CDK9 function during transcription restart after DNA repair. (A) Western blot showing the expression of CDK9 in MRC5 whole-cell extract after siRNA mediated knockdown of CDK9 in nonirradiated cells and 24h after irradiation. UBF serves as a loading control. (B) Quantification of at least three different experiments of CDK9 level normalized to UBF in nonirradiated cells and siCDK9 compared to siMock. (C and D) RNA synthesis in MRC5 cells after siRNA-mediated knockdown of the indicated factors in nonirradiated cells (C) and after UV-C exposure (D). At least 60 nuclei were analyzed. (E) Western blot showing the expression of CDK9 in MRC5 whole-cell extract after 6 h of treatment with CDK9 inhibitor (flavopiridol or iCDK9). UBF serves as a loading control. (F) RNA synthesis in MRC5 cells after 3 and 24 h of treatment with CDK9 inhibitor. At least 50 nuclei were analyzed. Error bars represent the standard errors of the mean (SEM). *P* values: *, <0.05; ***, <0.001.

quantifying the newly synthesized RNA via the incorporation of a fluorophore-coupled nucleoside analog. The experiment is conducted at different time points after UV induction (2, 5, 18, and 26 h), allowing quantifying the decline in transcriptional activity after UV damage (5 h after UV irradiation) and the restart of activity after repair of the DNA damage (18 h after UV irradiation). We used this test to quantify TCR activity in globally UV-irradiated siRNA-treated cells. Because CDK9 silencing might affect global transcription (15), we quantified the residual transcriptional activity during our experiments. We determined that 30% of the CDK9 protein is still present during the entire experiment time (0 to 24 h after irradiation) in the cells after silencing (Fig. 2A and B) and that this amount results in a 70% residual basal transcription activity (Fig. 2C).

In order to quantify only the effect of CDK9 silencing on TCR, we took into account the reduction in transcriptional activity observed when CDK9 is silenced and normalized the mRNA production at 2, 5, 18, and 26 h to the nonirradiated condition. As a positive control during RRS, CSB (an established repair factor, working specifically in TCR)-knocked-down cells have been used. As expected, in the absence of CSB, no restart of transcription after UV damage was observed. Knockdown of CDK9 resulted in a significantly reduced RNA synthesis at 18 h after UV, with a full recovery of RNA

synthesis at later time points (Fig. 2D), showing that the reduction of CDK9 retards the recovery of transcription after UV damage, affecting the TCR pathway (either retarding the repair reaction or delaying the restart of transcription after the completion of DNA repair). In the presence of the specific CDK9 inhibitors (16, 17) flavopiridol and iCDK9, although the amount of CDK9 was not affected (Fig. 2E), the amount of residual transcription was measured at 30% after 24 h of drug treatment (Fig. 2F). Such a low level of residual transcription is also observed after UV irradiation and for this reason did not permit the use of these drugs for transcription analysis.

CDK9 plays a role in the TCR reaction. In order to discriminate whether CDK9 plays a role in the repair process or in the restart of transcription after repair, we performed an assay designed previously in our group that specifically measures repair replication during TCR: the TCR-UDS assay (7). In addition, in order to verify that the effects measured in this assay are not an off-target effect of the CDK9 siRNAs pool, we stably expressed an siRNA-resistant FLAG-tagged murine CDK9 protein (CDK9^{siR}-FLAG) in GGR-deficient XPC (xeroderma pigmentosum complementation group C) mutant cells. We used a murine CDK9 because the amino acid sequences between human and murine CDK9 are very similar, whereas the nucleotide sequences are sufficiently different to confer resistance to human-raised siRNAs. We performed the TCR-UDS assay with two single siRNAs, si-CDK9-10 and siCDK9-11, and we could show that, in contrast to siCDK9-11, siCDK9-10 was effective in decreasing the levels of endogenous CDK9, whereas CDK9^{siR}-FLAG was not affected by the siCDK9-10 (Fig. 3A, bottom panel). In order to precisely localize the UV-induced DNA-damaged areas, a coimmunofluorescence labeling of γ -H2AX was performed, and repair replication was quantified. In siXPF-treated XPC-negative cells, both the GGR and the TCR pathways are compromised and, as expected, low TCR-UDS levels were observed (Fig. 3B, blue column). Knockdown of CDK9 (siCDK9-10, siCDK9-11, or siCDK9-pool) resulted in decreased TCR-UDS levels, although at levels that were intermediate between the siMock and siXPF (Fig. 3B). Interestingly, in the rescued cells expressing CDK9^{siR}-FLAG and not affected by siCDK9-10, TCR-UDS levels were fully restored (Fig. 3C, light green bar), demonstrating that CDK9 affects the TCR reaction.

In the presence of specific CDK9 inhibitors (16, 17), i.e., flavopiridol and iCDK9, the TCR-UDS was severely affected (Fig. 3D) at levels comparable to the ones measured in cells knocked down for XPF; nevertheless, this result is probably an indirect effect of the fact that these CDK9 inhibitors abolish CDK9 kinase activity and, in doing so, block the transcription reactions. Without transcription, no repair reactions (coupled to transcription) can be detected.

UV irradiation induces dissociation of the CDK9-HEXIM1 complex. In order to further study in details the role of CDK9 during TCR, we generated stably expressing green fluorescent protein (GFP)-tagged CDK9 (CDK9-GFP) MRC5 simian virus 40 (SV40)-immortalized human fibroblasts (here referred to as MRC5 cells). A simplified scheme of the recombinant fused protein is depicted in Fig. 4A. High-resolution confocal imaging of these cell lines revealed that CDK9-GFP is mainly present in the nucleoplasm and absent in the nucleoli and/or the cytoplasm (Fig. 4B). By performing immunofluorescence experiments on fixed cells exogenously expressing CDK9-GFP, we confirmed that the cellular localization of the recombinant protein is very similar to that of the endogenous proteins (Fig. 4B). Immunoblot analysis of whole-cell extracts of CDK9-GFP-expressing cells has been used to quantify the ratio of the recombinant protein expression in comparison to the endogenous untagged protein. As shown in Fig. 4C, CDK9-GFP expression is equivalent to the endogenous CDK9.

We could previously show that ELL is localized on locally damaged nuclear regions (7). Because of the physical interactions between ELL and CDK9 (11), we investigated whether CDK9 is also recruited on these damaged regions. We compared CDK9 immediate recruitment on DNA lesions to the accumulation of the TCR-specific Cockayne syndrome group A (CSA) protein (Fig. 4D). Confocal time-lapse images of living CDK9-GFP and CSA-GFP were taken after induction of local damage, and the accumu-

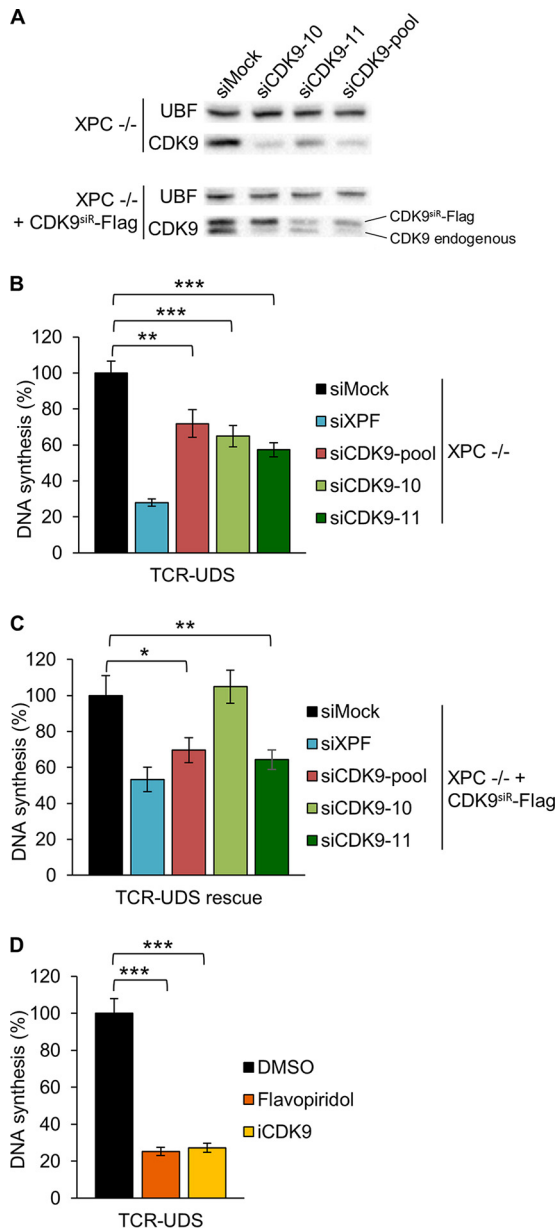


FIG 3 CDK9 function in TCR reaction. (A) Western blot showing the expression of CDK9 in whole-cell extract of XPC^{-/-} cell line (GGR-deficient cell line) and XPC^{-/-} cell line stably expressing a siRNA-resistant FLAG-tagged CDK9 protein (CDK9^{siR-Flag}) after siRNA-mediated knockdown of CDK9. UBF serves as a loading control. (B to D) TCR-UDS determined by EdU incorporation after local UV-C exposure in an XPC^{-/-} cell line (B) and an XPC^{-/-} cell line (C) stably expressing CDK9^{siR-Flag} after siRNA-mediated knockdown of the indicated factors or in an XPC^{-/-} cell line after CDK9 inhibitor treatment (D). At least 25 local damages were analyzed. Error bars represent the SEM. *P* values: *, <0.05; **, <0.01; and ***, <0.001.

lation of the two proteins on these locally damaged areas was quantified. Interestingly, in contrast to CSA and ELL (7), there was no accumulation of CDK9 to the DNA damage (Fig. 4D and E). This is not due to higher expression of the endogenous CDK9 compared to the GFP-tagged version, since their expression is equivalent, as shown above (Fig. 4C).

However, it should be noted that these recruitment measurements were obtained seconds after the induction of DNA damage. To quantify a possible recruitment of CDK9 on damaged DNA at later time points after UV irradiation, we utilized the Strip-FRAP (fluorescence recovery after photobleaching) method (18), in which fluorescent mole-

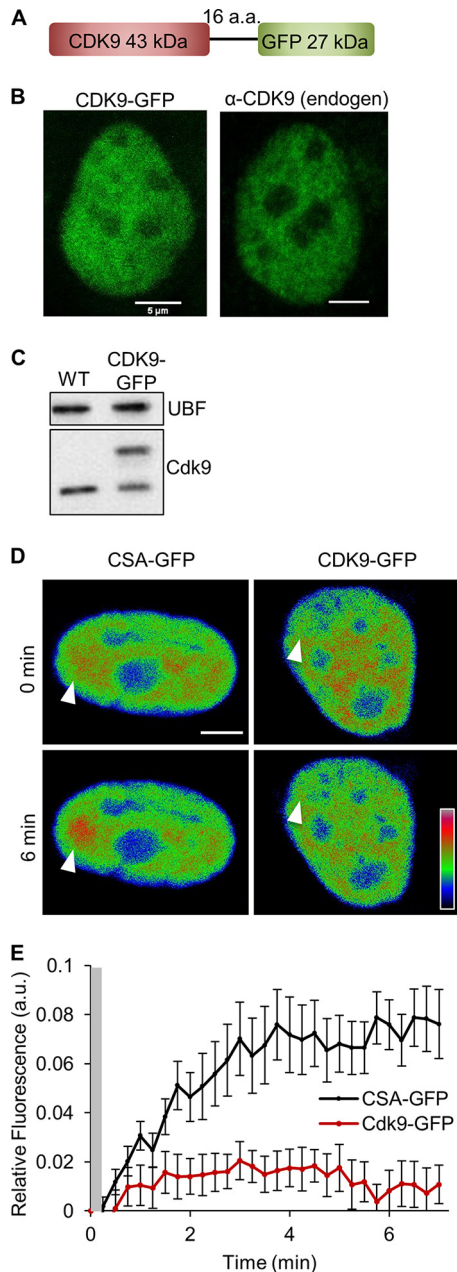


FIG 4 CDK9 dynamics during DNA damage response. (A) Scheme of the CDK9-GFP fusion protein. (B) Confocal images of CDK9-GFP-expressing cell lines and immunofluorescence staining of MRC5 cells with a primary antibody against CDK9. (C) Immunoblot probed with an anti-CDK9 antibody of WT MRC5 cells and MRC5 cells stably expressing CDK9-GFP. UBF serves as a loading control. (D) Confocal time-lapse images of a living mammalian fibroblast expressing CSA-GFP or CDK9-GFP, seen accumulating at a microirradiated area (arrows). Images were obtained using the Rainbow RGB lookup table. Scale bar, 5 μ m. (E) Accumulation curves of CDK9-GFP and CSA-GFP proteins at laser-induced DNA damage. The hatched region indicates the time window during which microirradiation-induced photobleaching masks the accumulation signal. Error bars represent the SEM obtained from at least 14 cells.

cules are photobleached in a small strip by a high-intensity laser pulse, and then the subsequent recovery of fluorescence is monitored over time within the bleached area. Without any damage, this measure of fluorescence recovery corresponds to the protein mobility within the living cell. However, when UV irradiation is applied, a protein that physically interacts with the damage is slowed down (due to the interactions with the substrate), and the recovery of fluorescence is reduced. Unexpectedly, as shown in Fig. 5A, instead of having a reduced mobility (as repair proteins have), CDK9 becomes more

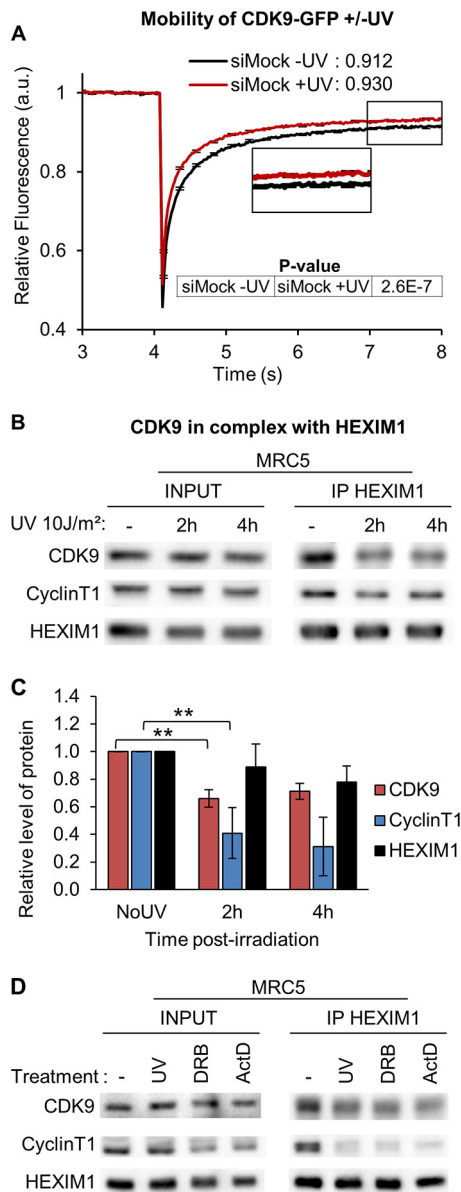


FIG 5 UV irradiation induces a dissociation of the CDK9-HEXIM1 complex. (A) Normalized FRAP analysis of CDK9-GFP-expressing cells after siRNA-mediated knockdown of the indicated factors. Cells were measured untreated (-UV) or 4 h after UV-C exposure (+UV). The average values between 7 and 8 s are indicated next to the graph legend. Error bars represent the SEM obtained from at least 27 cells from two independent experiments. The *P* values between two conditions are indicated in the table. (B and D) Immunoprecipitation of HEXIM1 in MRC5 cells treated with UV at different times (B) or treated with UV, DRB, or ActD for 2 h (D). Bound proteins were revealed by Western blotting with antibodies against cyclin T1, CDK9, and HEXIM1. INPUT, 20% of the lysate used for immunoprecipitation (IP) reactions. (C) Quantification of at least three different experiments (represented in panel B) of the IP/INPUT ratio compared to the no-UV-treatment (NoUV) condition. *P* value: **, <0.05.

mobile after UV irradiation. This might suggest the existence of fraction of CDK9 that is part of a larger complex with lower mobility, from which CDK9 dissociates upon UV-induced DNA damage in order to execute its specific role during the RTR process. In the absence of damage, CDK9 interacts physically with HEXIM1 (19), a subunit of the 7SK snRNP complex, which inhibits the kinase activity of CDK9 (19) within the P-TEFb complex. Because UV-dependent transcription inhibition induces a dissociation of P-TEFb from the 7SK snRNP complex (20), we wanted to confirm that in our experiments and, at the time points tested, CDK9's increased mobility, as measured by FRAP,

could be a result of the dissociation of CDK9 from HEXIM1. In order to verify this hypothesis, we immunoprecipitated HEXIM1 and quantified the amount of CDK9 and cyclin T1 found together with HEXIM1. As expected, in the absence of DNA damage HEXIM1 and CDK9/cyclin T1 could be coimmunoprecipitated (Fig. 5B and C). However, 2 to 4 h after UV irradiation, a smaller amount of CDK9/cyclin T1 could be immunoprecipitated, together with HEXIM1, showing, as previously reported (20) that UV irradiation causes a dissociation of CDK9/cyclin T1 from HEXIM1 (Fig. 5B and C). This dissociation is also observed when cells are treated with classical transcription inhibitors such as 5,6-dichloro-1- β -D-ribofuranosylbenzimidazole (DRB) or actinomycin D (ActD) (Fig. 5D), suggesting that this dissociation could be caused by transcription inhibition due to the RNAP2 stalling on UV lesions.

UV-dependent degradation of CDK9/cyclin T1 in the absence of CSB. To discriminate whether CDK9/HEXIM1 UV-dependent dissociation is due to a general transcription inhibition mechanism or whether it is specifically dependent on the TCR reaction, we measured CDK9 mobility upon UV damage in the absence of CSB (a TCR-deficient background). Interestingly, in the absence of CSB and after UV irradiation, transcription is permanently blocked (Fig. 2D) (21). However, the release of CDK9 from HEXIM1 upon UV induction is lost (Fig. 6A). This result was confirmed by immunoprecipitation assays, showing that in CSB depleted cells HEXIM1/cyclin T1/CDK9 are immunoprecipitated in the same proportions before and after UV damage (Fig. 6B and C). This UV-dependent dissociation can be explained by invoking that the remobilization from HEXIM1 of CDK9 after UV damage takes place via a CSB- and probably TCR-dependent mechanism or that the released fraction is rapidly degraded in the absence of CSB. This last hypothesis was confirmed by the fact that, unexpectedly, we noticed that after UV irradiation, in both CSB-deficient cells and CSB-knocked-down cells, the amounts of CDK9/cyclin T1 were consistently reduced compared to the amounts of HEXIM1 (Fig. 6D and E).

These combined results (FRAP and immunoprecipitation) demonstrate that after UV irradiation CDK9/cyclin T1 is released from the HEXIM1 complex, but when the DNA repair factor CSB is absent this free fraction is rapidly degraded after UV irradiation.

UV irradiation induces CSB-dependent RNAP2 serine 2 phosphorylation. During TCR, the first protein that encounters the lesion is the RNAP2. Not capable of bypassing the UV lesion, the RNAP2 is stalled and either backtracked or released from the substrate (22, 23). This transcriptional arrest triggers the TCR reaction. When DNA repair is efficiently performed, RNAP2 will be released from this arrest, and transcription will restart. Because this process is highly evocative of RNAP2 pausing downstream of promoters and CDK9 is involved in the phosphorylation and release of paused RNAP2 (24), we wanted to investigate whether, during TCR, RNAP2 was specifically phosphorylated. We examined Ser2, Ser5, and Ser7 RNAP2 phosphorylation (25, 26) after UV irradiation in wild-type (WT) cells 2 and 4 h after UV irradiation by performing Western blot analyses with nuclear extract; in this way, no cross-link could interfere with the accessibility of the epitope (27). Although there was no difference in Ser5 and Ser7 RNAP2 phosphorylation 2 h after UV irradiation, a well-defined increase in Ser2 RNAP2 phosphorylation was observed at this time point after UV damage induction (Fig. 7A and B). Interestingly, in CSB-knocked-down cells, this specific Ser2 RNAP2 is reduced (Fig. 7C and D), showing that this phosphorylation is indeed specific for TCR reactions. Surprisingly, CDK9-depleted cells presented a normal Ser2 RNAP2 phosphorylation 2 h after UV irradiation (Fig. 7E and F), demonstrating that CDK9 is not the kinase responsible for this phosphorylation. Because CDK12 can replace CDK9 for Ser2 phosphorylation (15, 28), we investigated whether the kinase activity of CDK12 could be responsible for this specific TCR Ser2 RNAP2 phosphorylation. CDK12-knocked-down cells were irradiated, and Ser2 RNAP2 phosphorylation was quantified 2 h after UV. Surprisingly, a reduction of CDK12 did not affect this TCR-specific RNAP2 phosphorylation (Fig. 7G and H). To confirm this result, we quantified the TCR-dependent Ser2 RNAP2 phosphorylation in cells depleted for the different cyclins associated with both CDK9

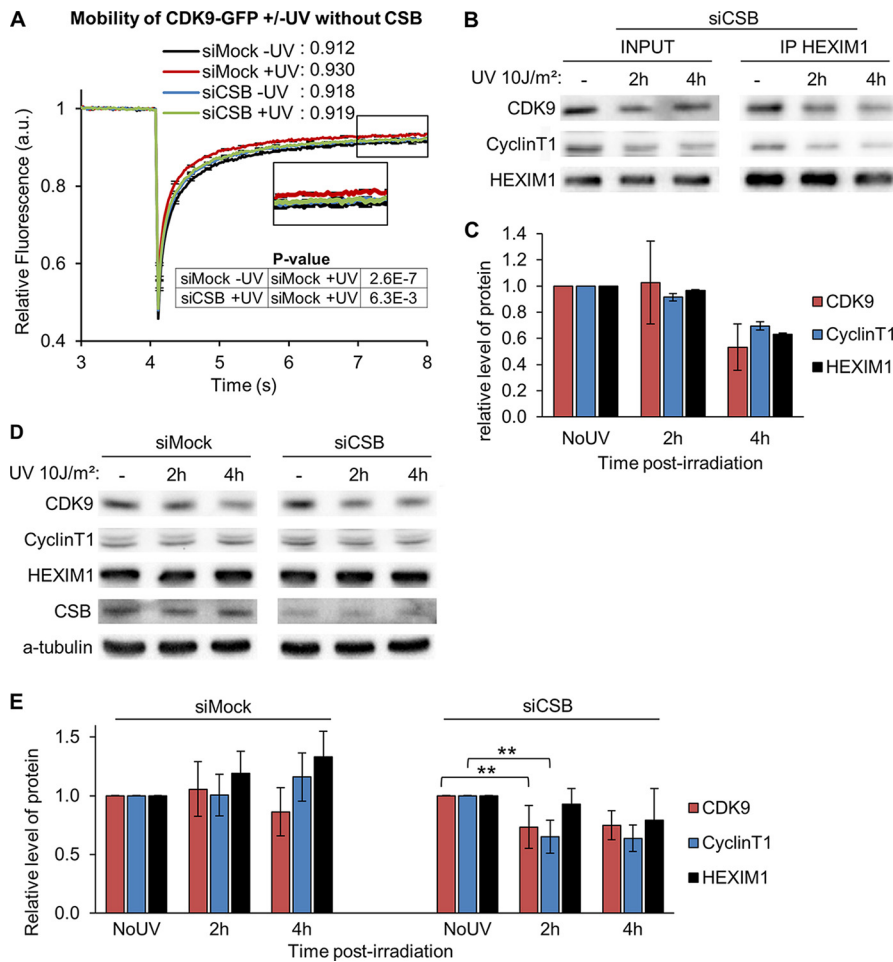


FIG 6 CDK9/cyclin T1 degradation without CSB. (A) Normalized FRAP analysis of CDK9-GFP stably expressed in MRC5 cells after siRNA-mediated knockdown of the indicated factors. Cells were measured untreated (-UV) or 4 h after UV-C exposure (+UV). The average values between 7 and 8 s are indicated next to the graph legend. Error bars represent the SEM obtained from at least 27 cells from two independent experiments. The *P* value between two conditions is indicated in the table. (B) Immunoprecipitation of HEXIM1 in MRC5 cells treated with siRNA against CSB, followed by different periods of irradiation. Bound proteins were revealed by Western blotting with antibodies against cyclin T1, CDK9, and HEXIM1. INPUT, 20% of the lysate used for IP reactions. (C) Quantification of at least two different experiments of the IP/INPUT ratio compared to the no-UV condition. (D) Immunoblot analysis of CDK9, cyclin T1, HEXIM1, and CSB in MRC5 cells treated with siRNA-mediated knockdown of the indicated factors, followed by different periods of irradiation. α -Tubulin serves as a loading control. (E) Quantification of Western blot analysis. The values of each protein are normalized to the no-UV condition. *P* value: **, <0.05.

and CDK12: cyclin K (Fig. 8A and B), cyclin T1 (Fig. 8C and D), cyclin T2 (Fig. 8E and F), and cyclins T1 and T2 (Fig. 8G and H). Our results show that none of these cyclins are associated with TCR-specific Ser2 RNAP2 phosphorylation (Fig. 8). Obviously, also in these experiments quantifications were normalized to the undamaged condition to be able to highlight exclusively the role of these kinases and cyclins after UV irradiation during the TCR reaction.

CDK9 increases the mobility of RNAP2 after UV irradiation. Because the kinase activity of CDK9 is not involved in the phosphorylation of RNAP2 during TCR, but having established that CDK9 plays a role in TCR (Fig. 3), we sought to investigate whether the absence of CDK9 would affect the mobility of the RNAP2 during the repair reaction. In order to answer this question, we produced a plasmid expressing a GFP-tagged version of RNAP2 (Fig. 9A) and stably transfected WT MRC5 cells. We could show that the GFP-Pol2 is localized in the nuclei of cells and excluded from the nucleolus, as endogenous RNAP2 (Fig. 9B). The GFP-Pol2 fusion protein is overex-

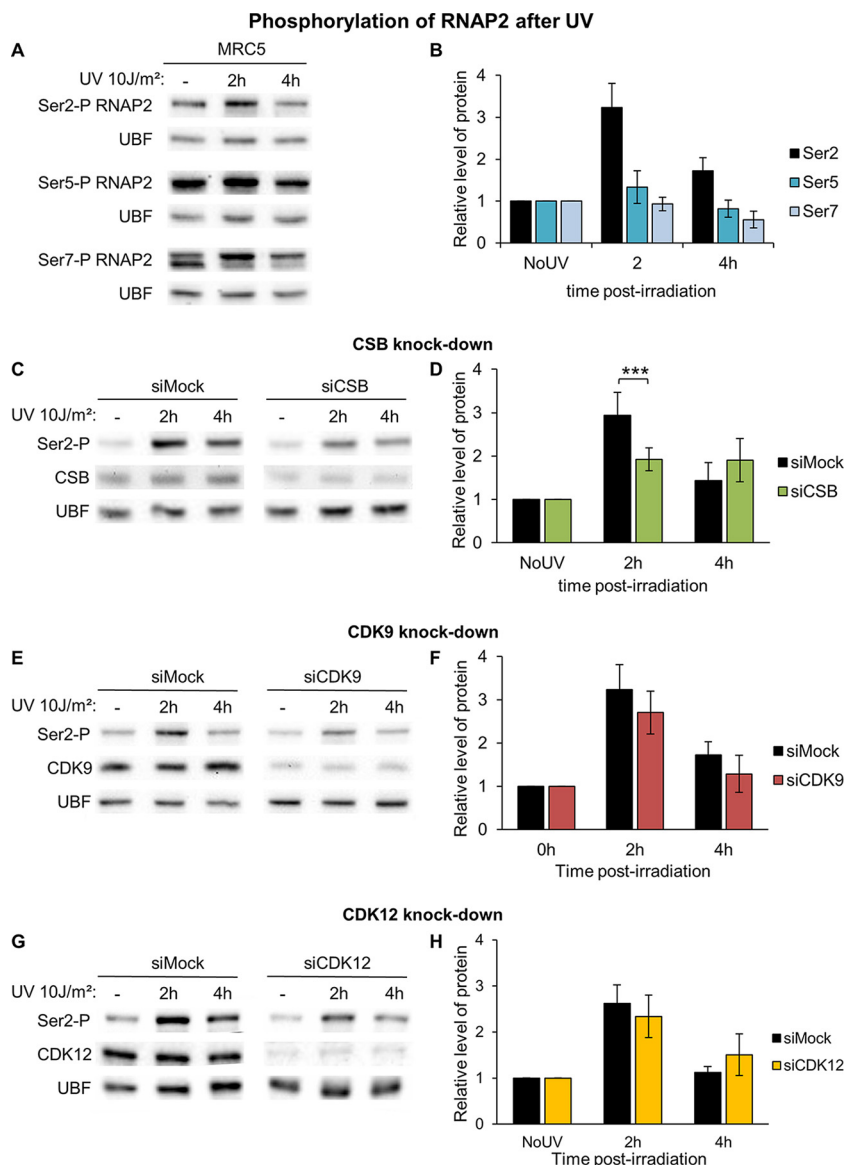


FIG 7 RNAP2 behavior in transcription restart after DNA damage. (A) Immunoblot showing the phosphorylation of Ser2, Ser5, or Ser7 of RNAP2 in MRC5 whole-cell extracts after UV irradiation. (B) Quantification of at least two different experiments of the RNAP2 phosphorylation/UBF ratio compared to the no-UV condition for each type of phosphorylation. (C, E, and G) Western blot showing the phosphorylation of Ser2 in MRC5 nuclear extract treated or not treated with UV-C after siRNA-mediated knockdown of the indicated factors showing the phosphorylation of Ser2. UBF serves as a loading control. (D, F, and H) Quantification of at least three different experiments of the RNAP2 phosphorylation/UBF ratio compared to the no-UV condition for each siRNA. *P* value: ***, <0.001.

pressed in the overall population of cells (Fig. 9C) and, for this reason, only low-expressing cells were chosen to perform FRAP analysis (Fig. 9D). Strip-FRAP assays showed that GFP-Pol2 is largely immobilized, showing only a limited fraction of recovered protein after the photobleaching. This immobile fraction represents the RNAP2 molecules engaged in the process of transcription and therefore retained on the chromatin. In order to verify this transcriptional engagement, we measured the mobility of RNAP2 after treatment with DRB, an inhibitor of RNAP2 transcription. After treatment, the immobile fraction of GFP-Pol2 was reduced, as also shown for other transcription factors (18, 29), indicating that the majority of GFP-Pol2 molecules are engaged toward the transcription process (Fig. 9E).

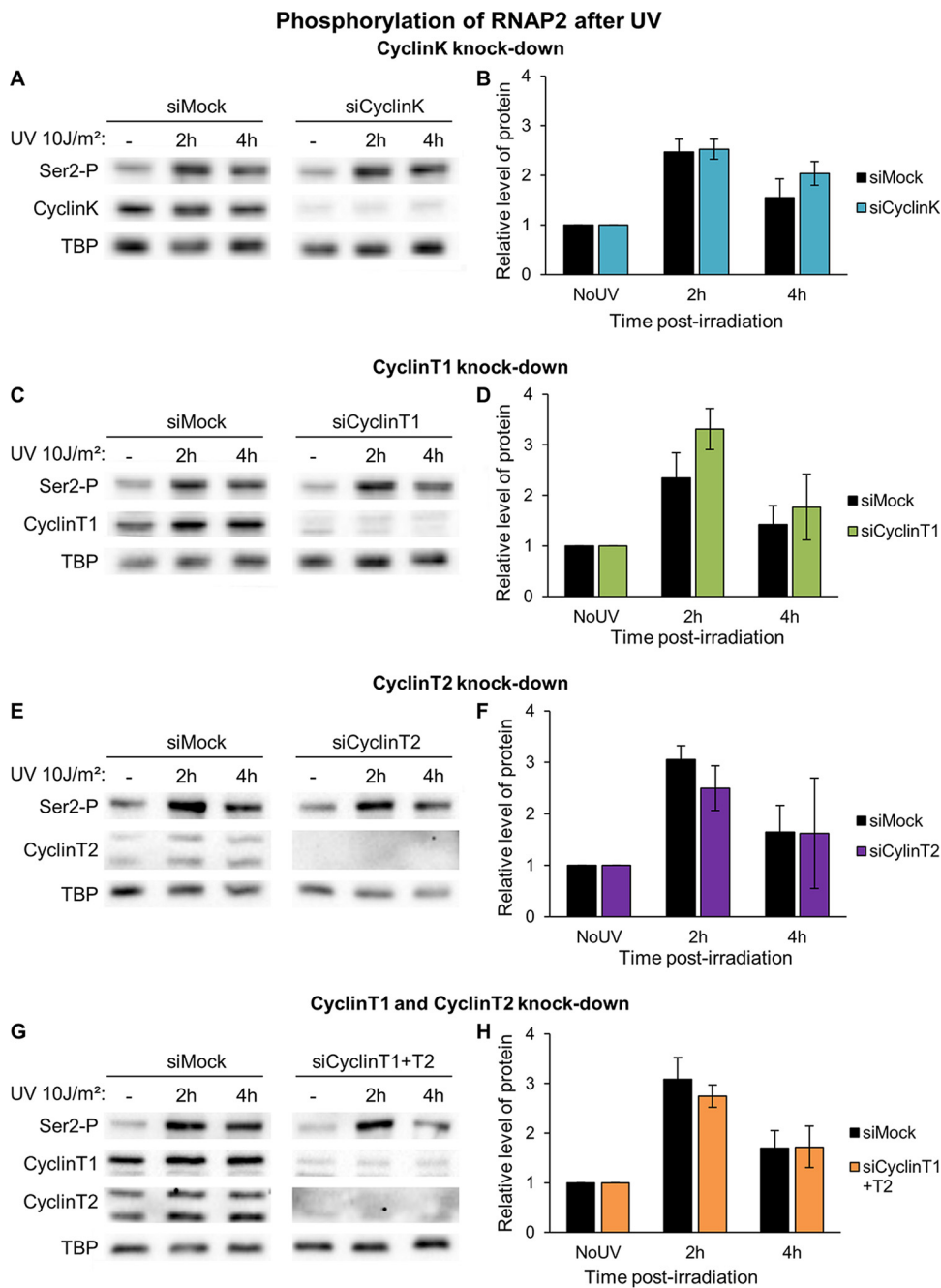


FIG 8 RNAP2 serine 2 phosphorylation without cyclin (K, T1, and T2) proteins. (A, C, E, and G) Western blot showing the phosphorylation of Ser2 in MRC5 nuclear extract treated or not treated with UV-C after siRNA-mediated knockdown of the indicated factors showing the phosphorylation of Ser2. TBP serves as a loading control. (B, D, F, and H) Quantification of at least two different experiments of the RNAP2 phosphorylation/TBP ratio compared to the no-UV condition for each siRNA.

To investigate the mobility of RNAP2 during TCR, we carried out Strip-FRAP experiments on GFP-Pol2-expressing cells in the presence or absence of UV damage. As already observed in a previous study by our group (7), there was no measurable change in the mobility of GFP-Pol2 after UV damage (Fig. 10A). This finding is explained by the fact that the majority of the RNAP2 immobile fraction is due to GFP-Pol2 molecules involved in transcription and that no additional measurable immobile fraction comes from lesion-stalled RNAP2 molecules.

However, in the absence of CDK9 and in the absence of DNA damage, the RNAP2 immobile fraction increases (Fig. 10B). This is probably due to the higher retention of

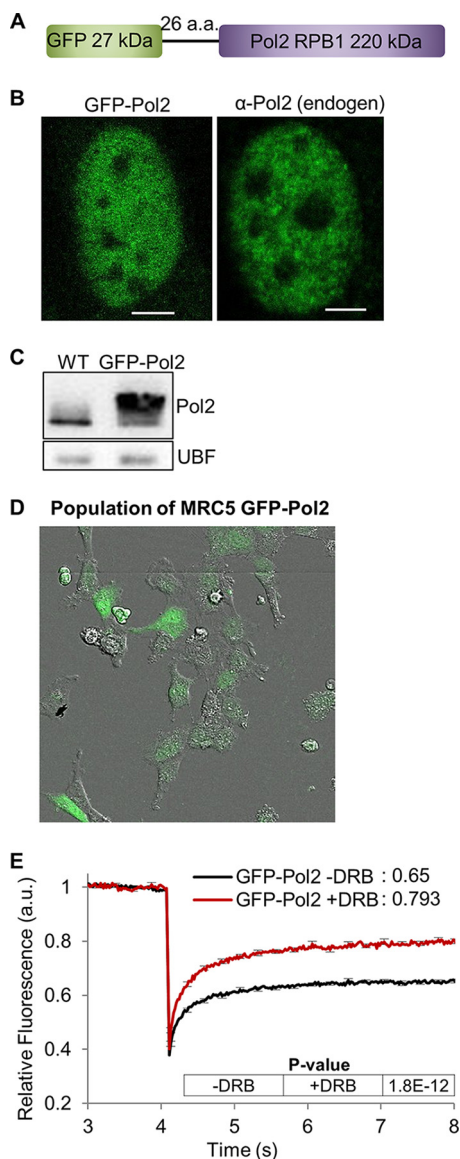


FIG 9 Characterization of cell lines stably expressing GFP-Pol2. (A) Scheme of the GFP-Pol2 fusion proteins. (B) Confocal images of GFP-Pol2-expressing cell lines and immunofluorescence staining of MRC5 cells with a primary antibody against total Pol2. Scale bar, 5 μ m. (C) Immunoblot probed with an anti-Pol2 antibody of WT MRC5 cells and MRC5 cells stably expressing GFP-Pol2. UBF serves as a loading control. (D) Confocal images of GFP-Pol2-expressing cell lines. Scale bar, 20 μ m. (E) FRAP analysis of GFP-Pol2-expressing cells either untreated (dark line) or treated with DRB (red line). The average values between 7 and 8 s are indicated next to the graph legend. Error bars represent the SEM obtained from at least 15 cells. The *P* value between the two conditions is indicated in the table.

RNAP2 molecules on transcriptional paused sites at proximal promoters, since CDK9 is essential for the RNAP2 release of paused sites and RNAP2 engagement in productive transcription elongation (30). The absence of CDK9, in combination with UV damage, results in an even more significant RNAP2 immobile fraction (Fig. 10C), indicating that there are more RNAP2 molecules retained on the chromatin (molecules stalled on UV lesions) in addition to the ones observed by default at the pausing sites.

DISCUSSION

Bulky DNA lesions distorting the DNA helix constantly challenge cell survival by interfering with and blocking cellular functions, such as replication and transcription. During evolution, cells have developed processes that counteract the deleterious effect

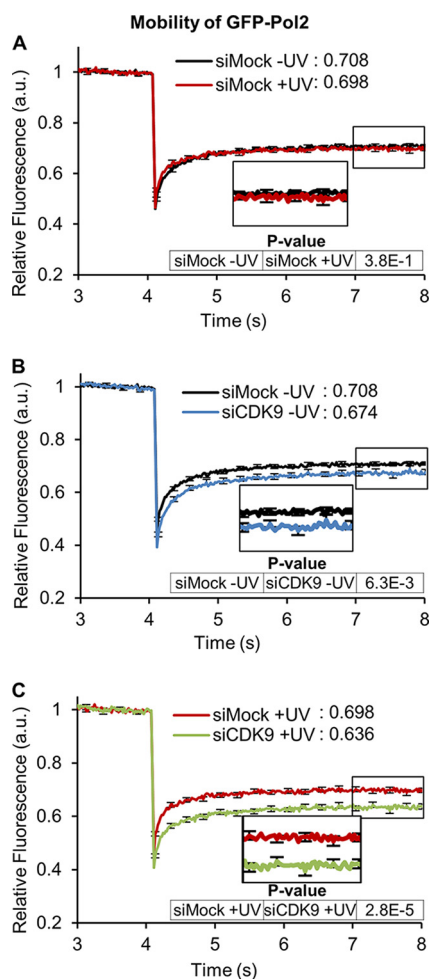


FIG 10 CDK9 increases the mobility of RNAP2 after UV irradiation. (A to C) Normalized FRAP analysis of GFP-Pol2-expressing cells after siRNA-mediated knockdown of indicated factors. Cells were measured either untreated (–UV) or 4 h after UC-C exposure (+UV). The average values between 7 and 8 s are indicated next to the graph legend. Error bars represent the SEM obtained from at least 27 cells from two independent experiments. The *P* value between the two conditions is indicated in the table.

of these damages, restoring an undamaged DNA molecule and allowing the restart of cellular processes. The importance of rapidly restoring cellular functions is better demonstrated by the existence of DNA repair processes tightly coupled with RNAP2 transcription. When bulky DNA damage, such as UV lesions, is located on the transcribed strands of active genes, RNAP2 is stalled, and transcription elongation is blocked. This pausing of transcription is necessary to allow the repair machineries to be recruited on the site of damage for the repair reaction to take place. Once the repair is completed, RNAP2 pausing may be released and transcription may restart.

During transcription and in the absence of any DNA damage, RNAP2 naturally pauses at promoter-proximal sites, 30 to 60 nucleotides downstream of the transcription start site (15). The release of this pausing into productive transcription elongation is under the control of P-TEFb, a heterodimeric cyclin-dependent kinase composed of CDK9 and cyclin T1/T2 (31). Because CDK9 interacts tightly with ELL and because ELL is involved in the RTR and is recruited to the damage via Cdk7 (7), we wondered whether CDK9 could play a role in RTR and, more importantly, whether RTR would share a molecular mechanism with the release of RNAP2 promoter-proximal pausing.

In the present study we focused on decrypting the role of CDK9 during TCR and RTR, since as well as for ELL (7), reduction of the CDK9 concentration in CDK9-knocked-down cells severely delays the RTR process (Fig. 2). In order to exclusively investigate the

effect of CDK9 reduction during RRS, we always normalized our results to the undamaged condition in which we determined that a 70% CDK9 reduction (obtained with several combinations of siRNAs) results in a 30% reduction in basal transcription activity. To investigate CDK9 action on damaged chromatin, we produced a GFP-labeled version of CDK9, and we quantified the mobility of CDK9-GFP before and after UV by using FRAP assays. During NER, the repair proteins are partially and temporarily immobilized on the damaged site, and this dynamic behavior influences the FRAP curves before and after UV irradiation. Namely, repair protein mobility is slower after UV damage (32). ELL was found to behave as a canonical repair protein, and the immobile fraction observed after DNA repair, as well as the immobilization on a locally damaged area, was comparable to the one measured for TCR-specific proteins, such as CSA (7). Surprisingly, CDK9 presented a different dynamic behavior after UV irradiation; instead of being more immobile, FRAP experiments pointed toward a remobilization of the protein. More remarkably, this remobilization was CSB dependent. To be able to fine-tune the RNAP2 pause release, CDK9 activity is kept under tight control by its interaction with a large inhibiting complex (7SK snRNP) (31). Indeed, activation of the CDK9/cyclin T implies a release from 7SK snRNP and in particular the dissociation from the P-TEFb inhibitor protein HEXIM1 (19). After UV irradiation, the increased mobility measured by FRAP analysis for CDK9 is concomitant with the dissociation of CDK9/cyclin T from HEXIM1 (Fig. 5). Surprisingly, after UV irradiation in CSB mutant cells and CSB-knocked-down cells, the amount of cellular CDK9/cyclin T is reduced. This novel observation points to a possible direct or indirect role of CSB in stabilizing the CDK9/cyclin T complex on the damaged site. In the absence of CSB, this stabilization is likely not achievable and the CDK9/cyclin T complex is degraded (Fig. 6). During TCR, it has been proposed that RNAP2 would backtrack and remain in the proximity of the damaged site to restart transcription (23) or that RNAP2 would detach from chromatin and restart transcription from the promoter (22, 33). It is possible that these processes could in fact coexist, depending on the site of damage (i.e., RNAP2 stalled at a lesion proximal to the initiation or termination would be more prone to disengage from the DNA) or the time it takes for the repair (i.e., longer repair timing could lead to RNAP2 disengagement). In both cases (at the site of damage or at the promoter), RNAP2 needs to restart the transcription, and this step requires phosphorylation of the CTD at one of the serines (2, 5, or 7). We could show here that, after UV irradiation and thus during TCR-RTR, RNAP2 is strongly phosphorylated at Ser2. Since phosphorylations can only occur when RNAP2 is bound to the DNA, we assume that this phosphorylation happens on RNAP2 chromatin-bound molecules. This Ser2 phosphorylation is specifically observed 2 h after UV irradiation and is less abundant at 4 h after irradiation. More interestingly, this Ser2 phosphorylation is specifically observed in TCR-proficient cells but absent, or greatly reduced, in TCR-deficient cells (Fig. 7), demonstrating that RNAP2 Ser2 phosphorylation is specifically needed for the restart of transcription after the completion of repair either from the promoter or from the site of damage. Surprisingly, we could demonstrate that CDK9 is not the kinase (nor is CDK12) that is in charge for this phosphorylation, which still takes place in CDK9- and CDK12-depleted cells (Fig. 7). This result was unexpected since it shows that the complex CDK9/cyclin T plays a different role in TCR-RTR than it does in the release of pausing at proximal promoters. Interestingly, CDK9 was necessary for proper TCR repair reactions (Fig. 3). Although we cannot say whether CDK9 kinase activity is necessary for the TCR reaction and while the substrate of a possible phosphorylation remains to be disclosed, our results show that, in contrast to RNAP2 promoter-proximal pausing, RNAP2 is not a CDK9 substrate during TCR (Fig. 7). To further investigate a possible role of CDK9 in RTR, we explored the effect of the absence of CDK9 on the mobility of RNAP2 molecules. In CDK9-knocked-down cells and without any damage, more RNAP2 molecules bind to the chromatin. This result is in accordance with the function of CDK9 during release of pausing, i.e., in its absence more RNAP2 molecules are paused on proximal promoters. However, after UV irradiation, an even further RNAP2 immobile fraction is observed in CDK9-knocked-down cells, supporting the hypothesis that without CDK9, RNAP2 is more bound to the

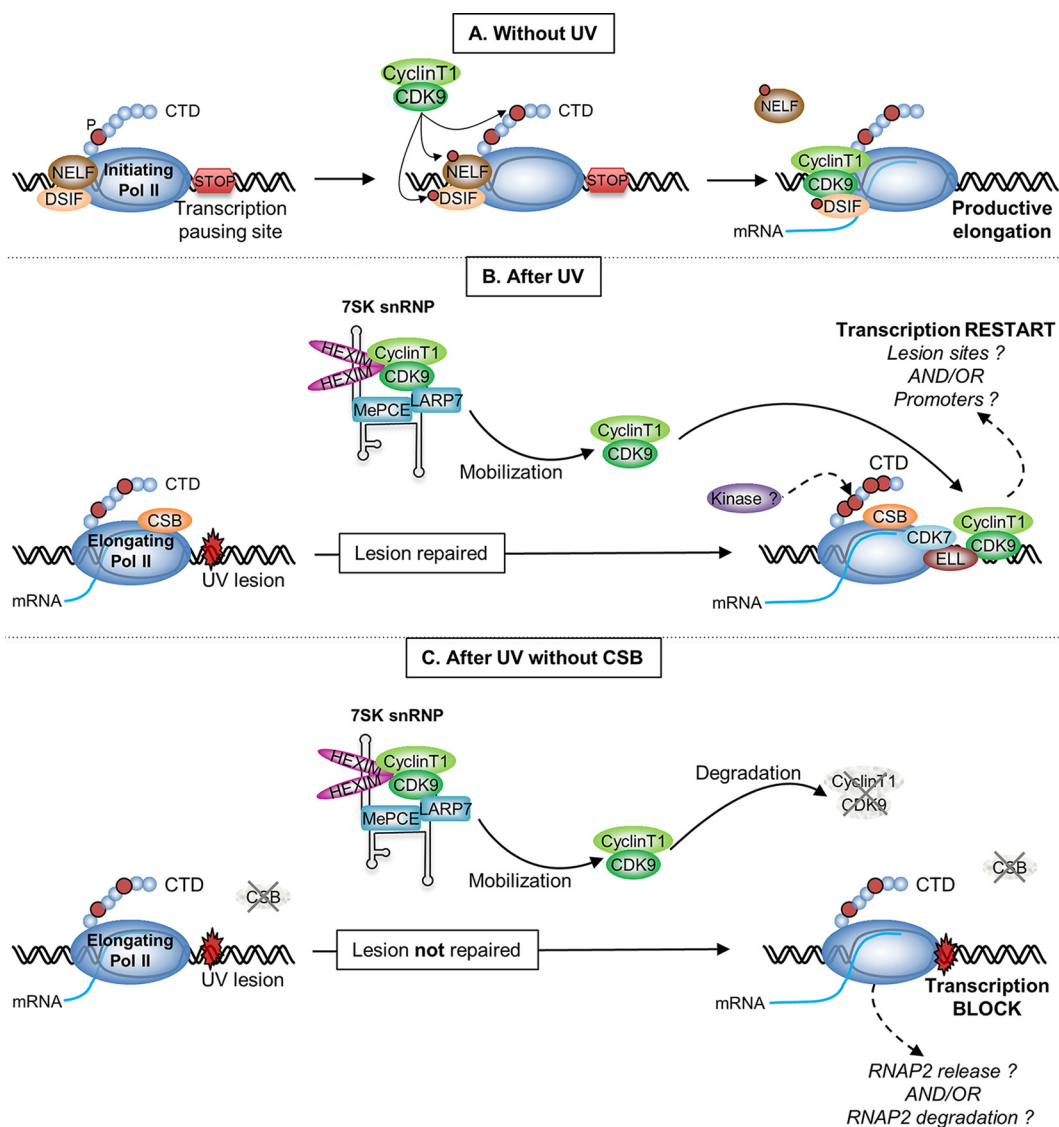


FIG 11 Mechanistic model of CDK9's role in DNA repair. (A) Immediately after initiation, RNAP2 enters transcriptional arrest mediated by DSIF and NELF. Their negative effect can be relieved by P-TEFb composed of CDK9 and cyclin T1. The kinase CDK9 phosphorylates (red circle) DSIF and NELF, as well as the Ser2 of the RNAP2 CTD, allowing productive elongation. (B) After UV irradiation, CDK9 and cyclin T1 are released from the 7SK snRNP complex and can be recruited to the site of damage probably via its interaction with ELL. After completion of the repair reaction (lesion removal and DNA gap filing), CDK9 plays an essential role to enable RNAP2 restart, probably by facilitating other proteins to be either recruited or stimulated in their function. (C) Without CSB, lesions are not repaired. CDK9/cyclin T1 are released from 7SK snRNP complex, and they are probably not recruited to the site of damage, leading to their rapid degradation. Transcription remains blocked, and RNAP2 is either released or degraded.

damaged chromatin and that the release of RNAP2 is impeded or at least retarded (Fig. 10). Interestingly, in our previous study, we observed that this increased RNAP2 immobile fraction is also observed when cells are ELL depleted (7). Our results could indicate that ELL and CDK9 play a structural role during RTR, facilitating other proteins to be either recruited or stimulated in their function of restarting transcription after completion of DNA repair. In conclusion, the role and mechanism of action of CDK9 is specific during TCR and RTR (Fig. 11, After UV) and is different from its function in the release of paused RNAP2 (Fig. 11, Without UV), indicating that although RTR and pausing might share common actors, the mechanism of action of RTR is unexpected and remains to be fully explored, starting from finding the kinase that is responsible for specific RNAP2 Ser2 phosphorylation.

MATERIALS AND METHODS

Cell culture. The cell strains used were in this study were as follows: (i) WT SV40-immortalized human fibroblasts (MRC5-SV), (ii) MRC5-SV stably expressing GFP-Pol II (G418 selected, 0.2 mg/ml), (iii) MRC5-SV stably expressing CDK9-GFP (G418 selected, 0.2 mg/ml), (iv) CSB-deficient SV40-immortalized human fibroblasts (CS1AN, TCR deficient), (v) MRC5-SV stably expressing CSA-GFP (G418 selected, 0.2 mg/ml), (vi) XPC-deficient SV40-immortalized human fibroblasts (XP4PA-SV, GGR deficient), and (vii) XP4PA-SV stably expressing an siRNA-resistant FLAG-CDK9 (hygromycin B selected, 50 μ g/ml). Human fibroblasts were cultured in a 1:1 mixture of Ham's F-10 and Dulbecco modified Eagle medium (Lonza) supplemented with antibiotics (penicillin and streptomycin) and 10% fetal calf serum at 37°C and 5% CO₂.

Specific treatment. DNA damage was inflicted by UV-C light (254 nm, 6-W lamp). For UV survival experiments, cells were exposed to different UV-C doses 1 day after plating. Survival was determined by clone counting 10 days after UV irradiation, as described previously (34). For the FRAP, RRS, and UDS experiments, cells were globally irradiated with 16 and 10 J/m² of UV-C for the immunoblot experiments, whereas for TCR-UDS the cells were locally irradiated with 100 J/m² m of UV-C through a 5- μ m-pore-size polycarbonate membrane filter (Millipore).

Cells were treated with 100 μ g/ml of 5,6-dichloro-1- β -D-ribofuranosylbenzimidazole (DRB; Sigma) or 2 μ g/ml of ActD for 2 h at 37°C before experiment (FRAP or immunoprecipitation). For CDK9 kinase inhibition, cells were treated with 0.5 μ M flavopiridol (Sigma, F3055) or 0.5 μ M iCDK9 (MedChemExpress, HY-16462/CS-1252).

Construction and expression of GFP-Pol 2 and CDK9-GFP fusion protein. Full-length RNAP2 c-DNA was cloned in-frame into pEGFP-C1 vector and full-length CDK9 c-DNA was cloned in-frame into pEGFP-N1 vector (Clontech). Constructs were sequenced prior to transfection. The plasmid siRNA-resistant CDK9 is a pCMV3 vector with full-length murine CDK9 c-DNA, FLAG-tagged in N-terminal (Sinobiological, HG 50897 NF). Transfection in MRC5-SV or XP4PA-SV cells was performed using Fugene transfection reagent (Roche). Stably expressing cells were selected with G418 (Gibco) or hygromycin B (Invitrogen), and fluorescent single cells were isolated after sorting using fluorescence-activated cell sorting (FACS-Calibur; Becton Dickinson).

Fluorescence recovery after photobleaching. FRAP experiments were performed as described previously (18) on a Zeiss LSM 710 NLO confocal laser scanning microscope (Zeiss), using a 40 \times /1.3-numerical-aperture (NA) oil objective, under a controlled environment (37°C, 5% CO₂). Briefly, a narrow region of interest (ROI) centered across the nucleus of a living cell was monitored every 20 ms (1% laser intensity of the 488-nm line of a 25-mW Argon laser) until the fluorescence signal reached a steady-state level (after ca. 2 s). The same strip was then photobleached for 20 ms at 100% laser intensity. Recovery of the fluorescence in the strip was then monitored (1% laser intensity) every 20 ms for about 20 s. Analysis of raw data were performed using ZEN software (Zeiss). All FRAP data were normalized to the average prebleached fluorescence after background removal. Every plotted FRAP curve is an average of at least 20 measured cells.

Laser microirradiation. In order to locally induce DNA damage in living cells, we used a tuneable near-infrared pulsed laser (Cameleon Vision II; Coherent, Inc.) directly coupled to an inverted confocal microscope equipped with a 40 \times /1.3-NA oil objective and a thermostatic chamber maintained at 37°C and 5% CO₂ (LSM 710 NLO; Zeiss). Typically, a small circular area (3 μ m in diameter) within the nucleus of a living cell was targeted three times to 15% of the laser (800 nm). Subsequent time-lapse imaging of targeted cells was performed every 15 s for 420 s. Image analysis was performed using ImageJ (W. S. Rasband, National Institutes of Health) and a custom-built macro, as follows: (i) the time series image stack was adjusted to compensate for cell movement (StackReg plugin), (ii) a ROI spanning the total nucleus was defined to compensate for unwanted photobleaching during the acquisition of images, and (iii) a "local damage" ROI was specified to quantify the fluorescence increase due to (GFP-tagged) protein recruitment at the laser-induced-DNA-damage area. At least 10 cells were measured for all cell lines.

RNA interference. The short interfering RNAs (siRNAs) used in this study are principally a pool of siRNAs: siMock, Dharmacon, D-001810-01 (10 nM); siCDK12, Santa Cruz, sc-44343 (5 nM); siCSB, Dharmacon, L-004888-00 (10 nM); siCyclin K, Dharmacon, L-029590-00 (10 nM); siCyclin T1, Dharmacon, L-003220-00 (10 nM); siCyclin T2, Dharmacon, L-003221-00 (10 nM); and siXPF, Dharmacon, M-019946-00 (10 nM). For siCDK9, the pool comprised Dharmacon L-003243-00 (10 nM), and two individual siRNAs from this pool were used: siCDK9-10, J-003243-10 (10 nM); and siCDK9-11, J-003243-11 (10 nM). The final concentration used for each siRNA is indicated in parentheses. Cells were transfected with siRNA using GenJET siRNA transfection reagent (Tebu-Bio) according to the manufacturer's protocol. Briefly, 100,000 cells were seeded per well of six-well plates and allowed to attach overnight. Transfection complexes were formed by 15 min of incubation at room temperature using buffer provided and added 24 h after seeding. A second siRNA transfection was performed 24 h after the first, and the cells were grown to confluence. Experiments were carried out 48 h after the first siRNA transfection. Protein knockdown was confirmed by Western blotting.

Protein extraction. For protein extraction, cells were cultured either in 10-cm dishes or in six-well plates if the cells had to be transfected with siRNA. Cells were harvested by trypsinization at the end of the experiment, after last time point of irradiation. When coverslips were used, the cells that remained in the dish once the coverslip was removed were collected.

The extraction of proteins has been performed using either a CellLytic NuCLEAR extraction kit (Sigma-Aldrich) for the nuclear extract or a mammalian cell lysis reagent kit (Sigma-Aldrich) for total protein extraction. The concentrations of proteins were determined by the Bradford method. The samples were then diluted with Laemmli buffer (10% glycerol, 5% β -mercaptoethanol, 3% sodium

dodecyl sulfate, 100 mM Tris-HCl [pH 6.8], bromophenol blue), heated to 95°C, and loaded on an SDS-PAGE gel.

Coimmunoprecipitation. For coimmunoprecipitation, 10 μ l of protein G-magnetic beads (Bio-ademead, Ademtech) was used for immunoprecipitation. Then, portions (1 μ g) of anti-HEXIM1 antibodies (rabbit, A303-113A; B ethyl) were bound to the beads in phosphate-buffered saline (PBS) with bovine serum albumin (5 mg/ml) for 2 h at 4°C with rotation. Next, 200 μ g of whole-cell extract was incubated with bead-antibody complex for 2 h at 4°C with rotation. After two washes with 100 mM salt, two washes with 150 mM salt, and one wash with 100 mM salt, the beads were boiled in 2 \times Laemmli buffer and loaded onto an SDS-PAGE gel.

SDS-PAGE. Proteins were separated using SDS-PAGE gel composed of bisacrylamide (37:5:1) and blotted onto a polyvinylidene difluoride membrane (0.45- μ m pore size; Millipore). Nonspecific sites were blocked in skimmed milk in the presence of 0.1% Tween 20, and the membrane was incubated with an appropriate antibody. We used the following antibodies: anti-serine 2 phosphorylation RNAP2 (rabbit, ab5095; Abcam); anti-serine 5 phosphorylation RNAP2 (rabbit, catalog no. 13523; Cell Signaling); anti-serine 7 phosphorylation RNAP2 (rabbit, catalog no. 13780; Cell Signaling); anti-RNAP2 (rabbit, sc-899; Santa Cruz Biotechnology); anti-CDK9 (rabbit, sc-8338X; Santa Cruz Biotechnology); anti-CSB (goat, sc10459; Santa Cruz Biotechnology); anti-cyclin K (rabbit, ab57311; Abcam); anti-cyclin T1 (rabbit, sc-10750 Santa Cruz Biotechnology); anti-cyclin T2 (mouse, ab50979; Abcam); anti-HEXIM1 (rabbit, A303-113A; B ethyl); anti- α -tubulin (mouse, T6074; Sigma-Aldrich); anti-UBF (mouse, sc-13125; Santa Cruz Biotechnology); and anti-TBP (mouse, 3TF1-3G3; Thermo Fisher). The loading was controlled with either anti-UBF, anti-TPB, or anti- α -tubulin antibody.

Protein bands were visualized via enhanced chemiluminescence (Pierce ECL Western blotting substrate) using horseradish peroxidase-conjugated secondary antibodies and imaged using the ChemiDoc system (Bio-Rad). The quantification of the band was performed with ImageLab software (Bio-Rad) using the method of volumes (rectangle). The background was removed using the local subtraction method.

RRS assays. MRC5-SV40 cells were grown on 24-mm coverslips. siRNA (siCDK9/siCSB) transfections were performed 24 and 48 h before the RRS assays. RNA detection was performed using a Click-iT RNA Alexa Fluor imaging kit (Invitrogen) according to the manufacturer's instructions. Briefly, cells were UV-C irradiated (16 J/m²) and incubated for 0, 3, 16, and 24 h at 37°C. For CDK9 inhibitor treatment, the cells were incubated for different times with the drugs. The cells were then incubated for 2 h with 5-ethynyl uridine, fixed, and permeabilized. Cells were incubated for 30 min with Click-iT reaction cocktail containing Alexa Fluor azide 488 or 594. After washing, the coverslips were mounted with Vectashield (Vector). Images of the cells were obtained with the same setup (see "Fluorescence recovery after photobleaching") and constant acquisition parameters, and then the average fluorescence intensity per nucleus was estimated after background subtraction (using ImageJ) and normalized to nontreated cells. For each sample, at least 80 nuclei were analyzed from three independent experiments.

Unscheduled DNA synthesis assays. MRC5-SV40 cells were grown on 24-mm coverslips. siRNA (siCDK9/siXPF) transfections were performed 24 h before the UDS assays. *De novo* DNA synthesis detection was performed using a Click-iT DNA Alexa Fluor imaging kit (Invitrogen) according to the manufacturer's instructions. Briefly, after global irradiation, the cells were incubated for 3 h with 5-ethynyl-2'-deoxyuridine (EdU), and then the cells were washed with PBS, fixed, and permeabilized. Fixed cells were incubated for 30 min with Click-iT reaction cocktail containing Alexa Fluor azide 594. After the washing step, the coverslips were mounted with Vectashield containing DAPI (4',6'-diamidino-2-phenylindole; Vector). Images of the cells were acquired, taking care not to take cells in replication. Images were analyzed as described for the RRS assay (see preceding paragraph). For each sample, at least 20 nuclei were analyzed from three independent experiments.

TCR-UDS assays: UDS measurement during TCR. XPC-deficient SV40-immortalized human fibroblasts (XP4PA-GGR-deficient cell line) were grown on 24-mm coverslips. siRNA (siCDK9/siXPF) transfections were performed 24 and 48 h before UDS assays and, for CDK9 kinase inhibition, drugs were added to the medium 2 h before irradiation. After local UV-C irradiation (100 J/m²) through a 5- μ m-pore-size polycarbonate membrane filter, the cells were incubated for 8 h with EdU (and CDK9 inhibitor), washed, fixed, and permeabilized. Fixed cells were treated with a PBS blocking solution (PBS+; PBS containing 0.15% glycine and 0.5% bovine serum albumin) for 30 min and then incubated with the primary mouse monoclonal antibody anti-yH2AX (Ser139 [Upstate, clone JBW301]) 1/500 diluted in PBS+ for 1 h, followed by extensive washes with Tween 20 in PBS. Cells were then incubated for 1 h with secondary antibodies conjugated to Alexa Fluor 488 fluorescent dye (Molecular Probes, 1:400 dilution in PBS+). The cells were then incubated for 30 min with Click-iT reaction cocktail containing Alexa Fluor azide 594. After a washing step, the coverslips were mounted with Vectashield containing DAPI. Images of the cells were obtained using the same microscopy system and constant acquisition parameters. Images were analyzed using ImageJ as follows: (i) a ROI outlining the locally damaged area was defined using yH2AX staining; (ii) a second ROI of comparable size was defined in the nucleus (avoiding nucleoli and other nonspecific signals) to estimate the background signal; and (iii) the "local damage" ROI was used to measure the average fluorescence correlated to EdU incorporation, which is an estimate of DNA replication after repair once the nuclear background signal obtained during step ii is subtracted. For each sample, between 50 and 60 nuclei were analyzed from three independent experiments.

Immunofluorescence. Cells were plated in 3.5-cm-diameter wells on 24-mm coverslips in order to reach 70% confluence on the day of the staining. Cells were washed twice in PBS, fixed in 2% paraformaldehyde, permeabilized two times for 10 min with PBS containing 0.1% Triton X-100 (PBS-T), and then washed with PBS containing 0.15% glycine and 0.5% bovine serum albumin (PBS+). We diluted antibodies in PBS+ and incubated cells with antibodies for 2 h at room temperature in a moist chamber.

Antibodies used were anti-CDK9 (rabbit, sc-484 [Santa Cruz Biotechnology], 1/500 dilution) and anti-RNA Pol II (rabbit, sc-899 [Santa Cruz Biotechnology], 1/500 dilution). After washing steps (three times, short wash; two times for 10 min each with PBS-T), the cells were incubated with secondary antibody coupled to fluorochrome (goat anti-rabbit antibody conjugated with Alexa Fluor 488 [A11088; Invitrogen], 1/500 dilution in PBS+). After the same washing procedure, coverslips were mounted with Vectashield containing DAPI (Vector). Slides were observed on a fluorescence microscope LSM710 NLO (Zeiss) using a 40×/1.3-NA objective, and the analysis was performed using ImageJ (NIH).

ACKNOWLEDGMENTS

We are grateful to Nicolas Heddebaut and Amandine Mourcet for technical assistance.

This study was supported by l'Agence Nationale de la Recherche (ANR DyReCT, ANR-14-CE10-0009) and the ARC (Association pour la Recherche sur le Cancer) foundation (projet Fondation ARC PJA 20131200188). L.-M.D. and G.S. were supported by l'Agence Nationale de la Recherche (ANR DyReCT, ANR-14-CE10-0009). A.L. was supported by Association pour la Recherche sur le Cancer (postdoctoral grant).

The funders had no role in study design, data collection and analysis, decision to publish, or preparation of the manuscript.

REFERENCES

- Giglia-Mari G, Zotter A, Vermeulen W. 2011. DNA damage response. *Cold Spring Harb Perspect Biol* 3:a000745. <https://doi.org/10.1101/cshperspect.a000745>.
- Hanawalt PC. 1994. Transcription-coupled repair and human disease. *Science* 266:1957–1958. <https://doi.org/10.1126/science.7801121>.
- Donahue BA, Yin S, Taylor JS, Reines D, Hanawalt PC. 1994. Transcript cleavage by RNA polymerase II arrested by a cyclobutane pyrimidine dimer in the DNA template. *Proc Natl Acad Sci U S A* 91:8502–8506. <https://doi.org/10.1073/pnas.91.18.8502>.
- Fousteri M, Vermeulen W, van Zeeland AA, Mullenders LH. 2006. Cockayne syndrome A and B proteins differentially regulate recruitment of chromatin remodeling and repair factors to stalled RNA polymerase II *in vivo*. *Mol Cell* 23:471–482. <https://doi.org/10.1016/j.molcel.2006.06.029>.
- Fousteri M, Mullenders LH. 2008. Transcription-coupled nucleotide excision repair in mammalian cells: molecular mechanisms and biological effects. *Cell Res* 18:73–84. <https://doi.org/10.1038/cr.2008.6>.
- Oksenyich V, Zhovmer A, Ziani S, Mari PO, Eberova J, Nardo T, Stefanini M, Giglia-Mari G, Egly JM, Coin F. 2013. Histone methyltransferase DOT1L drives recovery of gene expression after a genotoxic attack. *PLoS Genet* 9:e1003611. <https://doi.org/10.1371/journal.pgen.1003611>.
- Mourgues S, Gautier V, Lagarou A, Bordier C, Mourcet A, Slingerland J, Kaddoum L, Coin F, Vermeulen W, Gonzales de Peredo A, Monsarrat B, Mari PO, Giglia-Mari G. 2013. ELL, a novel TFIIH partner, is involved in transcription restart after DNA repair. *Proc Natl Acad Sci U S A* 110:17927–17932. <https://doi.org/10.1073/pnas.1305009110>.
- Dinant C, Ampatzidis-Michaïlidis G, Lans H, Tresini M, Lagarou A, Grosbart M, Theil AF, van Cappellen WA, Kimura H, Bartek J, Fousteri M, Houtsmuller AB, Vermeulen W, Marteijn JA. 2013. Enhanced chromatin dynamics by FACT promotes transcriptional restart after UV-induced DNA damage. *Mol Cell* 51:469–479. <https://doi.org/10.1016/j.molcel.2013.08.007>.
- Adam S, Polo SE, Almouzni G. 2013. Transcription recovery after DNA damage requires chromatin priming by the H3.3 histone chaperone HIRA. *Cell* 155:94–106. <https://doi.org/10.1016/j.cell.2013.08.029>.
- Kong SE, Banks CA, Shilatfard A, Conaway JW, Conaway RC. 2005. ELL-associated factors 1 and 2 are positive regulators of RNA polymerase II elongation factor ELL. *Proc Natl Acad Sci U S A* 102:10094–10098. <https://doi.org/10.1073/pnas.0503017102>.
- Lin C, Smith ER, Takahashi H, Lai KC, Martin-Brown S, Florens L, Washburn MP, Conaway JW, Conaway RC, Shilatfard A. 2010. AFF4, a component of the ELL/P-TEFb elongation complex and a shared subunit of MLL chimeras, can link transcription elongation to leukemia. *Mol Cell* 37:429–437. <https://doi.org/10.1016/j.molcel.2010.01.026>.
- Price DH. 2008. Poised polymerases: on your mark...get set...go. *Mol Cell* 30:7–10. <https://doi.org/10.1016/j.molcel.2008.03.001>.
- Byun JS, Fufa TD, Wakano C, Fernandez A, Haggerty CM, Sung MH, Gardner K. 2012. ELL facilitates RNA polymerase II pause site entry and release. *Nat Commun* 3:633. <https://doi.org/10.1038/ncomms1652>.
- Buratowski S. 2009. Progression through the RNA polymerase II CTD cycle. *Mol Cell* 36:541–546. <https://doi.org/10.1016/j.molcel.2009.10.019>.
- Bowman EA, Kelly WG. 2014. RNA polymerase II transcription elongation and Pol II CTD Ser2 phosphorylation: a tail of two kinases. *Nucleus* 5:224–236. <https://doi.org/10.4161/nucl.29347>.
- Morales F, Giordano A. 2016. Overview of CDK9 as a target in cancer research. *Cell Cycle* 15:519–527. <https://doi.org/10.1080/15384101.2016.1138186>.
- Lu H, Xue Y, Yu GK, Arias C, Lin J, Fong S, Faure M, Weisburd B, Ji X, Mercier A, Sutton J, Luo K, Gao Z, Zhou Q. 2015. Compensatory induction of MYC expression by sustained CDK9 inhibition via a BRD4-dependent mechanism. *Elife* 4:e09993. <https://elifesciences.org/articles/06535>.
- Giglia-Mari G, Miquel C, Theil AF, Mari PO, Hoogstraten D, Ng JM, Dinant C, Hoeijmakers JH, Vermeulen W. 2006. Dynamic interaction of TTDA with TFIIH is stabilized by nucleotide excision repair in living cells. *PLoS Biol* 4:e156. <https://doi.org/10.1371/journal.pbio.0040156>.
- Kobbi L, Demey-Thomas E, Braye F, Proux F, Kolesnikova O, Vinh J, Poterszman A, Bensaude O. 2016. An evolutionary conserved Hexim1 peptide binds to the Cdk9 catalytic site to inhibit P-TEFb. *Proc Natl Acad Sci U S A* 113:12721–12726. <https://doi.org/10.1073/pnas.1612331113>.
- Yang Z, Zhu Q, Luo K, Zhou Q. 2001. The 7SK small nuclear RNA inhibits the CDK9/cyclin T1 kinase to control transcription. *Nature* 414:317–322. <https://doi.org/10.1038/35104575>.
- Epanchintsev A, Costanzo F, Rauschendorf MA, Caputo M, Ye T, Donnio LM, Proietti-de-Santis L, Coin F, Laugel V, Egly JM. 2017. Cockayne's syndrome A and B proteins regulate transcription arrest after genotoxic stress by promoting ATF3 degradation. *Mol Cell* 68:1054–1066.e6. <https://doi.org/10.1016/j.molcel.2017.11.009>.
- Chiou YY, Hu J, Sancar A, Selby CP. 2018. RNA polymerase II is released from the DNA template during transcription-coupled repair in mammalian cells. *J Biol Chem* 293:2476–2486. <https://doi.org/10.1074/jbc.RA117.000971>.
- Pani B, Nudler E. 2017. Mechanistic insights into transcription coupled DNA repair. *DNA Repair (Amst)* 56:42–50. <https://doi.org/10.1016/j.dnarep.2017.06.006>.
- Schuller R, Forne I, Straub T, Schrieck A, Texier Y, Shah N, Decker TM, Cramer P, Imhof A, Eick D. 2016. Heptad-specific phosphorylation of RNA polymerase II CTD. *Mol Cell* 61:305–314. <https://doi.org/10.1016/j.molcel.2015.12.003>.
- Hsin JP, Xiang K, Manley JL. 2014. Function and control of RNA polymerase II C-terminal domain phosphorylation in vertebrate transcription and RNA processing. *Mol Cell Biol* 34:2488–2498. <https://doi.org/10.1128/MCB.00181-14>.
- Jeronimo C, Collin P, Robert F. 2016. The RNA polymerase II CTD: the increasing complexity of a low-complexity protein domain. *J Mol Biol* 428:2607–2622. <https://doi.org/10.1016/j.jmb.2016.02.006>.

27. Mayer A, Lidschreiber M, Siebert M, Leike K, Soding J, Cramer P. 2010. Uniform transitions of the general RNA polymerase II transcription complex. *Nat Struct Mol Biol* 17:1272–1278. <https://doi.org/10.1038/nsmb.1903>.
28. Bartkowiak B, Liu P, Phatnani HP, Fuda NJ, Cooper JJ, Price DH, Adelman K, Lis JT, Greenleaf AL. 2010. CDK12 is a transcription elongation-associated CTD kinase, the metazoan ortholog of yeast Ctk1. *Genes Dev* 24:2303–2316. <https://doi.org/10.1101/gad.1968210>.
29. Hoogstraten D, Nigg AL, Heath H, Mullenders LH, van Driel R, Hoeijmakers JH, Vermeulen W, Houtsmuller AB. 2002. Rapid switching of TFIIH between RNA polymerase I and II transcription and DNA repair *in vivo*. *Mol Cell* 10:1163–1174. [https://doi.org/10.1016/S1097-2765\(02\)00709-8](https://doi.org/10.1016/S1097-2765(02)00709-8).
30. Jonkers I, Kwak H, Lis JT. 2014. Genome-wide dynamics of Pol II elongation and its interplay with promoter proximal pausing, chromatin, and exons. *Elife* 3:e02407. <https://doi.org/10.7554/eLife.02407>.
31. Nguyen VT, Kiss T, Michels AA, Bensaude O. 2001. 7SK small nuclear RNA binds to and inhibits the activity of CDK9/cyclin T complexes. *Nature* 414:322–325. <https://doi.org/10.1038/35104581>.
32. Rademakers S, Volker M, Hoogstraten D, Nigg AL, Mone MJ, Van Zeeland AA, Hoeijmakers JH, Houtsmuller AB, Vermeulen W. 2003. Xeroderma pigmentosum group A protein loads as a separate factor onto DNA lesions. *Mol Cell Biol* 23:5755–5767. <https://doi.org/10.1128/MCB.23.16.5755-5767.2003>.
33. Ghosh-Roy S, Das D, Chowdhury D, Smerdon MJ, J Smerdon M, Chaudhuri RN. 2013. Rad26, the transcription-coupled repair factor in yeast, is required for removal of stalled RNA polymerase II following UV irradiation. *PLoS One* 8:e72090. <https://doi.org/10.1371/journal.pone.0072090>.
34. Jensen A, Mullenders LH. 2010. Transcription factor IIS impacts UV-inhibited transcription. *DNA Repair (Amst)* 9:1142–1150. <https://doi.org/10.1016/j.dnarep.2010.08.002>.